Observations of [O I] emission in Comets C/2014 Q2 (Lovejoy) and C/2007 N3 (Lulin): Possible Influence of Solar Activity on Oxygen Line Ratios

ELLA J. MAYFIELD $^{\bigcirc}$, ADAM J. MCKAY $^{\bigcirc}$, MICHAEL S. P. KELLEY $^{\bigcirc}$, AND ANITA L. COCHRAN $^{\bigcirc}$ 3

¹Department of Physics and Astronomy, Appalachian State University, 525 Rivers St., Boone, NC 28607 ²Department of Astronomy, University of Maryland, 4296 Stadium Dr., College Park, MD 20742, USA

ABSTRACT

Observing [O I] emission to calculate an "oxygen line ratio" has been proposed as a potential proxy for direct CO₂ measurement in comets. However, the photochemistry governing [O I] release into the coma is not well understood, and using theoretical release rates often yields different results than using empirical release rates determined in conjunction with direct space-based measurements of CO₂. We hypothesize that the accuracy of the release rates could depend on the level of solar activity at the time the comet is observed, which will be influenced by the solar cycle. We present observations and analysis of [O I] emission in one comet observed near solar maximum, C/2014 Q2 (Lovejoy), and one near solar minimum, C/2007 N3 (Lulin). Our [O I] measurements were obtained using two high spectral resolution optical spectrographs: the Tull Coudè spectrometer at McDonald Observatory and the ARCES spectrometer at Apache Point Observatory. We use empirical and theoretical models for [O I] emission from the literature to derive multiple sets of inferred CO₂ abundances for these comets and compare to contemporaneous space-based measurements of CO₂. We find that the empirical model, which was developed based on comet observations obtained near solar maximum, reproduces the directly measured CO₂ abundances better for Lovejoy. Neither model accurately reproduces the direct measurement for Lulin. We discuss the implications of our findings for the accuracy and dependencies of the oxygen line ratio method for inferring CO₂ abundances in cometary comae.

Keywords: Comets (280) — Comae (271)

1. INTRODUCTION

Comets formed during the earliest stages of the solar system, and have undergone very little heating or processing since they were formed. This means their composition provides a unique window into the physical and chemical conditions present during the early era of solar system formation. Specifically, studying the volatile composition of comets is crucial to understanding both current cometary activity and evolutionary processes. The primary volatiles present in most comets are H₂O, CO₂, and CO, and these species are widely considered the drivers of cometary activity. Therefore, studying the sublimation behavior of these species is paramount to understanding cometary activity.

Both H_2O and CO are directly observable from the ground using near-infrared measurements, and CO is also observable in the sub-millimeter. However, the only direct method for measuring CO_2 is through the v_3 band at $4.26 \ \mu m$, which

can only be observed using space-based facilities due to severe telluric absorption at this wavelength. Observing time on space-based facilities is often limited, so a ground-based proxy for direct $\rm CO_2$ measurement is of extreme importance. Since atomic oxygen is a photodissociation product of $\rm H_2O$, $\rm CO_2$, and $\rm CO$, observations of the forbidden oxygen lines at 5577, 6300, and 6364Å can serve as a proxy for direct measurement of these species.

Photodissociation of H_2O , CO_2 , and CO causes the release of oxygen atoms in an excited state, either 1S or 1D , depending on the wavelength of the incident photon. These atoms will then radiatively de-excite through the 5577Å line (1S) or 6300 and 6364Å lines (1D). Water releases oxygen atoms in the 1S state at 3-8% the rate that it releases atoms in the 1D state, while CO_2 and CO release $O(^1S)$ at 30-90% the rate of release of $O(^1D)$ (A. Delsemme 1980; M. C. Festou & P. D. Feldman 1981; A. Bhardwaj & S. Raghuram 2012). This difference is reflected in the ratio of the line intensities (hereafter referred to as the "oxygen line ratio"), which is given

Email: may fielde j@app state.edu, mckay aj@app state.edu

³Department of Astronomy, University of Texas at Austin, 2515 Speedway, Austin, Texas, 78712*

^{*} McDonald Observatory

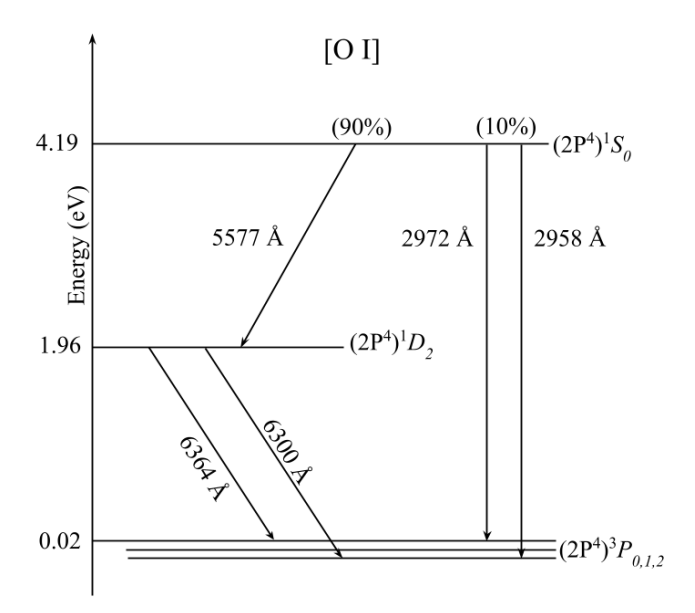


Figure 1. Energy level diagram for atomic oxygen [O I]. In analysis of the oxygen line ratio, the 2972 and 2958Å lines can be ignored as they only comprise 10% of transitions from the ^{1}S level to the ^{1}D level. Note that all atoms that decay through the 5577Å line will then also decay through either the 6300 or 6364Å line. Figure adapted from A. Bhardwaj & S. Raghuram (2012).

by:

$$R \equiv \frac{N(O(^{1}S))}{N(O(^{1}D))} = \frac{I_{2958} + I_{2972} + I_{5577}}{I_{6300} + I_{6364}}$$
(1)

where N(x) represents the column density of the species x and I_{y} represents the intensity of line y. Since the 2958 and 2972Å lines are much fainter than the others (10% of the 5577Å line) and are unobservable from the ground, they are often ignored in calculations of the oxygen line ratio (T. G. Slanger et al. 2011), although one could also incorporate a correction factor for their absence into calculations of the $\frac{CO_2}{H_2O}$ ratio (see section 2.1.3). For low number densities where collisional quenching is not significant, the oxygen line ratio will always be less than one, because any atom that decays through the 5577Å line will then also decay through either the 6300 or 6364Å line (shown in Figure 1, the energy level diagram for [O I]). If water is the dominant parent molecule, the oxygen line ratio calculated should be 0.03-0.08, whereas if CO₂ or CO dominates, the oxygen line ratio should be 0.3-0.9 (A. Delsemme 1980; M. C. Festou & P. D. Feldman 1981; A. Bhardwaj & S. Raghuram 2012).

This qualitative method of determining the dominant parent molecule has been well-established, but in recent years it has been suggested that the oxygen line ratio could also be used quantitatively to infer a relative abundance of CO_2 to H_2O (A. J. McKay et al. 2012, 2013, 2015, 2016; A. Decock et al. 2013). However, this is only valid if the photochemistry governing [O I] release is well understood. De-

spite attempts to develop and constrain [O I] release rates in the laboratory, using these rates often produces discrepancies with direct measurements of CO_2 abundances from spacecraft, and empirical release rates determined in conjunction with these space-based measurements are often able to more accurately reproduce the directly measured $\frac{CO_2}{H_2O}$ ratio (A. J. McKay et al. 2012, 2013, 2015, 2016). However, empirical release rates (such as those developed by A. J. McKay et al. (2015)) only succeed at reproducing these direct measurements for some comets and not others (e.g., A. McKay et al. 2020; K. Hall et al. 2021).

One potential factor that could be contributing to the discrepancies between theoretical and empirical release rates and their accuracy is the level of solar activity at the time of observation. The release of oxygen atoms into the coma is caused by photodissociation of the parent molecule by ultraviolet wavelengths of sunlight. The ultraviolet spectrum of the sun varies in spectral shape and intensity over the solar cycle. This variable behavior across a solar cycle could have an effect on the photochemistry of [O I] release and may explain the discrepancies found between sets of release rates in the literature.

We present observations and analysis of the forbidden oxygen lines at 5577, 6300, and 6364Å in one comet observed near solar maximum, C/2014 Q2 (hereafter "Lovejoy"), and one near solar minimum, C/2007 N3 (hereafter "Lulin"). We use both the theoretical release rates from A. Bhardwaj & S. Raghuram (2012) and the empirical release rates established by A. J. McKay et al. (2015) to derive inferred CO₂ abundances for these comets and compare to contemporaneous space-based measurements of CO₂ obtained with the Spitzer Space Telescope (Lovejoy, this work) and AKARI spacecraft (Lulin, T. Ootsubo et al. 2012). We describe our observations and our data reduction and analysis procedures in Section 2. Section 3 presents our measured oxygen line ratios and a comparison of our inferred CO2 abundances with the abundances measured by Spitzer and AKARI. Section 4 discusses the implications of our results in relation to the oxygen line ratio's potential dependence on the solar cycle. In Section 5 we summarize our conclusions and suggest future work.

2. OBSERVATIONS AND DATA ANALYSIS

2.1. Optical observations

We obtained spectra of both Lovejoy and Lulin across multiple dates. Table 1 provides the observation dates and geometries. The majority of the data were obtained using the Tull Coudé spectrograph mounted on the 2.7-meter Harlan J. Smith Telescope at McDonald Observatory. The Tull Coudé provides a spectral resolving power of $R \equiv \frac{\lambda}{\Delta\lambda} = 60000$ and a spectral range from 3500-10000Å. Although this range contains interorder gaps redward of 5800Å, we were careful to set the grating such that the red oxygen lines (6300 and

6364Å) were fully covered by our observations. The size of the slit on the sky is $1.2^{\circ} \times 8.2^{\circ}$. Other specifications concerning the Tull Coudé spectrograph can be found in A. Cochran (2001); R. G. Tull et al. (1995). An additional night of observations for Lovejoy was obtained three months after the initial observations using the ARCES echelle spectrograph on the 3.5-meter Astrophysical Research Consortium Telescope at Apache Point Observatory. ARCES provides a spectral resolving power of R = 31500 and a spectral range 3500-10000Å. This range contains no interorder gaps. The projected size of the slit on the sky is $3.2^{\circ} \times 1.6^{\circ}$. Other specifications concerning the ARCES spectrograph can be found in S.-i. Wang et al. (2003), A. J. McKay et al. (2012), and A. J. McKay et al. (2013).

We centered the slit on the optocenter of the comet for all observations, barring one spectrum of Lovejoy that was obtained at an offset position 100" tailward on February 3 (see Section 4 for discussion of this spectrum). We utilized an ephemeris from JPL Horizons to track the optocenter's apparent motion across the sky. The guiding software employs a boresight technique, which keeps the slit on the optocenter by monitoring optocenter flux that falls outside the slit. In order to correct for solar absorption and continuum features caused when comet dust reflects sunlight, a solar analog star (HD245) was observed for the ARCES data. Observing a solar standard star was not necessary for the Tull Coudé data, as the Tull Coudé spectrograph possesses a solar port that feeds in sunlight directly from the daytime sky, from which we could obtain an observed solar spectrum to correct for solar features. For most nights, we observed a fast-rotating (vsin(i) > 150 km/s) O, B, or A star to correct for telluric features in the spectra. If it was not possible to observe a fast rotator due to clouds or other hindrances, the fast rotator spectrum from the previous or following night was used when correcting for telluric features. For photometric nights, observations of a flux standard star were obtained, providing a means for absolute flux calibration for those nights. Table 1 lists the calibration stars observed and indicates whether conditions were photometric for each night. Spectra of a quartz lamp and ThAr lamp were also obtained for flat fielding and wavelength calibration, respectively.

2.1.1. Data reduction

We reduced and extracted the spectra using Image Reduction and Analysis Facility (IRAF) scripts that carry out bias subtraction, cosmic ray removal, flat fielding, and wavelength calibration procedures. To remove telluric features, we divided the comet, solar, and flux standard spectra by the fast rotator spectrum. For photometric nights, we used the flux standard spectrum to convert the tellurically corrected comet spectrum flux to physical units. We shifted the tellurically corrected solar spectrum in wavelength and scaled

it vertically to align with the flux-calibrated comet spectrum. We then subtracted this shifted, scaled solar spectrum from the comet spectrum to correct for solar absorption features and remove Fraunhofer lines and the continuum level.

For spectrographs with narrow slit widths such as Tull Coudé and ARCES, it is necessary to estimate how much flux was lost falling outside of the slit during observations of the flux standard star. As a best practice, we incorporate a slit loss correction factor into analysis of all of our data. For observations of Lovejoy, we were able to find the transmittance through the slit by performing aperture photometry on the slit viewer images as described in A. J. McKay et al. (2014). Estimates of 75-90% are typical for the transmittance, with a typical standard deviation in this estimate of around 10%. Therefore, we adopt a 10% uncertainty in our absolute flux calibration measurements (and therefore our water production rates). For observations of Lulin, slit viewer images were not available, so the slit loss correction was an estimate based on the average seeing, which was ~ 0.5 .

2.1.2. Deblending of telluric and cometary lines

The forbidden oxygen lines at 5577, 6300, and 6364Å also occur as telluric emission features, meaning that a combination of a large geocentric velocity (and therefore a large Doppler shift) and high spectral resolution are necessary to separate the cometary and telluric lines. For almost all of the observations, the geocentric velocity was high enough that the cometary and telluric features were completely separated. However, for the May observations of Lovejoy, there was enough overlap between the lines that deblending them became necessary. Each line profile is determined by the instrumental point spread function because the line widths are unresolved. The instrumental point spread function is described well by a Gaussian for our spectra. We fit the observed line profile to the sum of two Gaussians (one corresponding to the cometary line and the other to the telluric line) using the Python package pyspeckit's function Spectrum. A full description of the deblending process can be found in A. J. McKay et al. (2012). Figure 2 shows an example spectrum with this deblending method applied and the resulting curve fits constructed graphically.

2.1.3. Data analysis

The ratio of the 6300Å line flux to the 6364Å line flux reflects the branching ratio of the two respective transitions from the ¹D energy level to the ³P ground state (see Figure 1). This ratio is well established as 3.0 (P. J. Storey & C. J. Zeippen 2000; B. D. Sharpee & T. G. Slanger 2006; A. Cochran 2001; A. L. Cochran 2008; A. J. McKay et al. 2012, 2013; A. Decock et al. 2013). We confirmed that our data reproduced this accepted ratio within uncertainty before proceeding with further analysis. After this was confirmed, we used the measured line fluxes to calculate the oxygen line ratio, simplified

Table 1. Optical observation log. For non-photometric nights, the spectrum of the flux standard star from either the previous or following night was used. However, because all lines are measured simultaneously, whether the night was photometric does not affect the ratio of the fluxes (i.e. the measured oxygen line ratios).

Object	Date (UT)	r(AU)	$\Delta (AU)$	$\dot{\Delta}$ (km/s)	Instrument	Solar standard	Fast Rot.	Flux Cal.	Photometric?
Lovejoy	2015 Feb 02	1.29	0.79	32.9	Tull Coudè	Solar port	HR 838	•••	No
	2015 Feb 03 ^a	1.29	0.81	33.2	Tull Coudè	Solar port	HR 628	HR 3454	Yes
	2015 Feb 04	1.29	0.83	33.4	Tull Coudè	Solar port			No
	2015 May 11	1.95	2.16	12.7	ARCES	HR 245	HR 333	HR 5501	Yes
Lulin	2009 Feb 14	1.32	0.56	-43.4	Tull Coudè	Solar port			No
	2009 Feb 15	1.33	0.54	-41.1	Tull Coudè	Solar port	HR 4875	HR 4875	Yes

^a Note: one of the spectra obtained on February 3 was obtained at an offset position 100" tailward; see Section 4 for analysis of this spectrum.

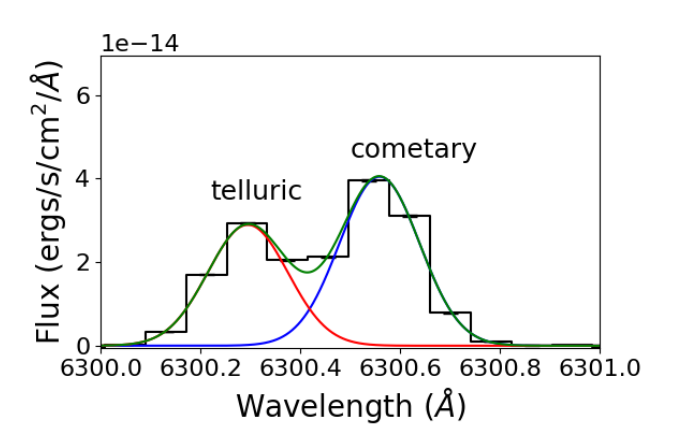


Figure 2. Region of the spectrum obtained of Lovejoy on UT May 11, 2015 that contains the forbidden oxygen line at 6300Å. Note that the cometary line appears redward of 6300Å due to Doppler shifting caused by the comet's geocentric velocity. The data are represented by a histogram (black) with 1σ errorbars. The data are fitted with two separate Gaussians corresponding to the telluric (red) and cometary (blue). The sum of the two Gaussian components is plotted in green.

from Equation 1 to be:

$$R = \frac{I_{5577}}{I_{6300} + I_{6364}} \tag{2}$$

The ratio of CO₂ to H₂O can be derived by observing that each species' contribution of line flux can be expressed as the product of the release rate W and the column density N. Substituting these expressions for the line fluxes into Equation 2 and solving for $\frac{N_{CO_2}}{N_{H_2O}}$ produces the following equation (A. J. McKay et al. 2012; A. Decock et al. 2013):

$$\frac{N_{CO_2}}{N_{H_2O}} = \frac{RW_{H_2O}^{red} - W_{H_2O}^{green} - W_{CO}^{green} \frac{N_{CO}}{N_{H_2O}} + RW_{CO}^{red} \frac{N_{CO}}{N_{H_2O}}}{W_{CO_2}^{green} - RW_{CO_2}^{red}}$$
(3)

where N_x represents the column density of species x and R represents the oxygen line ratio from Equation 2. The release rate W is defined as

$$W = \tau^{-1} \alpha \beta \tag{4}$$

Table 2. [O I] release rates for H_2O and CO_2 for the 1S and 1D electron states. Column 3 lists empirical release rates (B) from A. J. McKay et al. (2015), while Column 4 lists theoretical release rates from A. Bhardwaj & S. Raghuram (2012).

Parent	[O I] State	McKay2015	B&R2012
		$(10^{-8} \ s^{-1})$	$(10^{-8} \ s^{-1})$
H ₂ O	^{1}S	0.64	2.6
H_2O	^{1}D	84.4	84.4
CO_2	^{1}S	50.0	72.0
CO ₂	^{1}D	75.0	120.0

where τ is the parent molecule's photodissociative lifetime, α is the yield into the excited state of interest, and β is a given line's branching ratio out of a certain excited state. Each instance of W in Equation 3 specifies both the line in question (red or green, corresponding to the 6300/6364Å "red doublet" or the 5577Å "green line", respectively) and the parent molecule. We scale the release rate for ${}^{1}S$ (the green line) by 0.9 to account for the 10% of atoms that de-excite through the unobservable 2972 and 2958Å lines. In this work we use both theoretical release rates from A. Bhardwaj & S. Raghuram (2012) and empirical release rates from A. J. McKay et al. (2015) (from which we use release rates "B", as this set seemed to prove more accurate when utilized by A. J. McKay et al. (2016)) to infer CO₂ abundances from our oxygen line ratio measurements in order to evaluate the accuracy of both sets of release rates when used for objects observed at different levels of solar activity (see Table 2 for numerical values of these release rates).

Although other, more complex molecules containing oxygen (e.g. H_2CO , CH_3OH) are present in cometary comae, they are much less abundant than H_2O , CO_2 , and CO, and they release oxygen through a multi-step process. This makes contribution to the [O I] population from these molecules very inefficient, and we consider this contribution negligible for our analysis. There is also some precedent for considering the contribution of CO photodissociation to the [O I] population to be negligible (S. Raghuram &

A. Bhardwaj 2014; S. Raghuram et al. 2020), which is a reasonable assumption for our data due to the small measured $\frac{CO}{H_2O}$ ratios for Lovejoy and Lulin reported in other works (N. Dello Russo et al. 2022; E. L. Gibb et al. 2012). Applying this assumption, Equation 3 simplifies to:

$$\frac{N_{CO_2}}{N_{H_2O}} = \frac{RW_{H_2O}^{red} - W_{H_2O}^{green}}{W_{CO_2}^{green} - RW_{CO_2}^{red}}$$
(5)

The relationships given in Equations 3 and 5 are independent of heliocentric distance (A. J. McKay et al. 2013, 2015, 2016).

For small fields of view (which applies to both our ARCES and Tull Coudé data), the column density ratio from Equation 5 reflects the production rate ratio (see A. J. McKay et al. (2015) and references therein for more details). A small field of view can also increase the importance of accounting for the preferential collisional quenching of ¹D atoms (corresponding to the 6300 and 6364Å lines) over ¹S atoms (corresponding to the 5577Å line) (A. Bhardwaj & S. Raghuram 2012; S. Raghuram & A. Bhardwaj 2014; A. Decock et al. 2014). The oxygen line ratio used in the previous equations are calculated under the assumption that collisional quenching did not affect the line fluxes, which is likely untrue. Thus, the observed fluxes for the 6300 and 6364Å lines need to be increased to account for the ${}^{1}D$ atoms that were present in the coma but de-excited through collisions instead of emitting photons (and therefore do not contribute to the intensities of the observed emission lines). The dominant molecule contributing to collisions is H₂O, so to estimate the amount of collisional quenching in an observation, we must estimate the H₂O production rate.

H₂O production rates were determined with our 6300Å observations using the Haser model (L. Haser 1957) and other established algorithms described in A. J. McKay et al. (2012, 2015). We adopt an expansion velocity following the relation from A. L. Cochran & D. G. Schleicher (1993); S. A. Budzien et al. (1994):

$$v = (0.85 \text{ km s}^{-1}) r^{-0.5}$$
 (6)

where r is the heliocentric distance of the comet in units of AU. The algorithms employed produce a correction factor that scales the observed flux to the expected theoretical flux without collisional quenching. This correction factor is then applied to our oxygen line ratio measurements.

To ensure that the uncertainties in [O I] photochemistry do not affect the derived water production rates, we compared our results with other measurements of water production rates for Lovejoy and Lulin obtained around the same dates as our own observations (see Section 4). Additionally, using the 6300Å line flux has been well established as a proxy for obtaining water production rates (J. P. Morgenthaler et al. 2001, 2007; U. Fink 2009; A. J. McKay et al.

2015; A. J. McKay et al. 2018, 2021). The original and corrected oxygen line ratios are presented in Section 3 along with our water production rates.

2.2. Infrared observations

Observations of comet Lovejoy were obtained with the Spitzer Space Telescope (M. W. Werner et al. 2004) as part of the Cometary Orbital Trends with Spitzer survey (program IDs 11106 and 13116; M. S. Kelley et al. 2017). Images were obtained with the InfraRed Array Camera (IRAC) instrument, which is comprised of four 256×256 pixel arrays (1"22 per pixel) in the focal plane, each with their own broadband filter (G. G. Fazio et al. 2004). Observations were obtained after Spitzer's cryogens were depleted, and were limited to two bandpasses: 3.6 μ m and 4.5 μ m. The comet was observed on three dates near perihelion, which occurred on 2015 January 30 at 01:40 UTC (JPL Horizons solution #59). The observational circumstances are presented in Table 3. The telescope followed the comet with its non-sidereal rates, and mapped the coma with a 3×3 array pattern with 260" steps (84% of the array size). The two detector arrays observe independent locations on the sky separated by 91"; therefore, the pattern was offset in such a way to enable efficient mapping of the comet with a single observing sequence. At each position in the pattern, 5 images were taken, each with random offsets to reduce noise and improve scene sampling (IRAC's "cycling" dither pattern with a medium scale; S. Laine 2010). Two exposures were taken at each position with 0.4 and 10.4 s exposure times, but the longer exposures saturated at 4.5 µm so we limited our analysis to the short exposure data. To measure the background, the observing sequences were re-executed at the same location on the sky, including non-sidereal rates, after the comet had moved out of the mapped area.

Raw images were processed with version S19.2.0 of the IRAC pipeline to produce flux calibrated images and downloaded from the Spitzer Heritage Archive (IRSA 2022). We use the pipeline's "corrected" data products, which have been produced to address several common artifacts: stray light, multiplexer striping, column pull down, and banding (internal optical scattering). The individual images were combined in the rest frame of the comet by date, exposure time, and bandpass using the MOPEX software (D. Makovoz & I. Khan 2005). After subtracting the shadow mosaics from the target mosaics, residual background was measured in an area clear of the comet and removed. The resulting images of the comet are presented in Fig. 3.

IRAC's broadband filters may include significant contributions from dust (scattered light and/or thermal emission), and gas, especially CO₂ at 4.26 μ m and CO at 4.67 μ m (W. T. Reach et al. 2013). The gas can be isolated by scaling the 3.6 μ m image to match the dust brightness in the 4.5 μ m

Table 3. Observational circumstances and photometric data for the Spitzer Space Telescope and AKARI data sets.

Comet	Telescope	Date	r	Δ	$F_{V}(3.6)^{a}$	$F_{V}(4.5)^{a}$	$C_{\mathrm{dust}}^{\ \ b}$	$Q(CO_2)$	Reference
		(UTC)	(AU)	(AU)	(Jy)	(Jy)		(10^{28} s^{-1})	
Lulin	AKARI	2009 Feb 05 00:34	1.275	0.817				0.485 ± 0.049	Ootsubo et al. 2012
Lovejoy	Spitzer	2015 Feb 17 03:28	1.319	0.974	2.37 ± 0.07	9.99 ± 0.30	2.84	4.95 ± 0.15	This work
	Spitzer	2015 Feb 27 15:19	1.360	1.002	2.21 ± 0.07	$\boldsymbol{9.02 \pm 0.27}$	2.65	5.15 ± 0.15	
	Spitzer	2015 Mar 13 04:08	1.436	1.130	1.59 ± 0.05	6.41 ± 0.19	2.24	5.69 ± 0.17	

^aNot color corrected. ^bDust 3.6-to-4.5 μm scale factor.

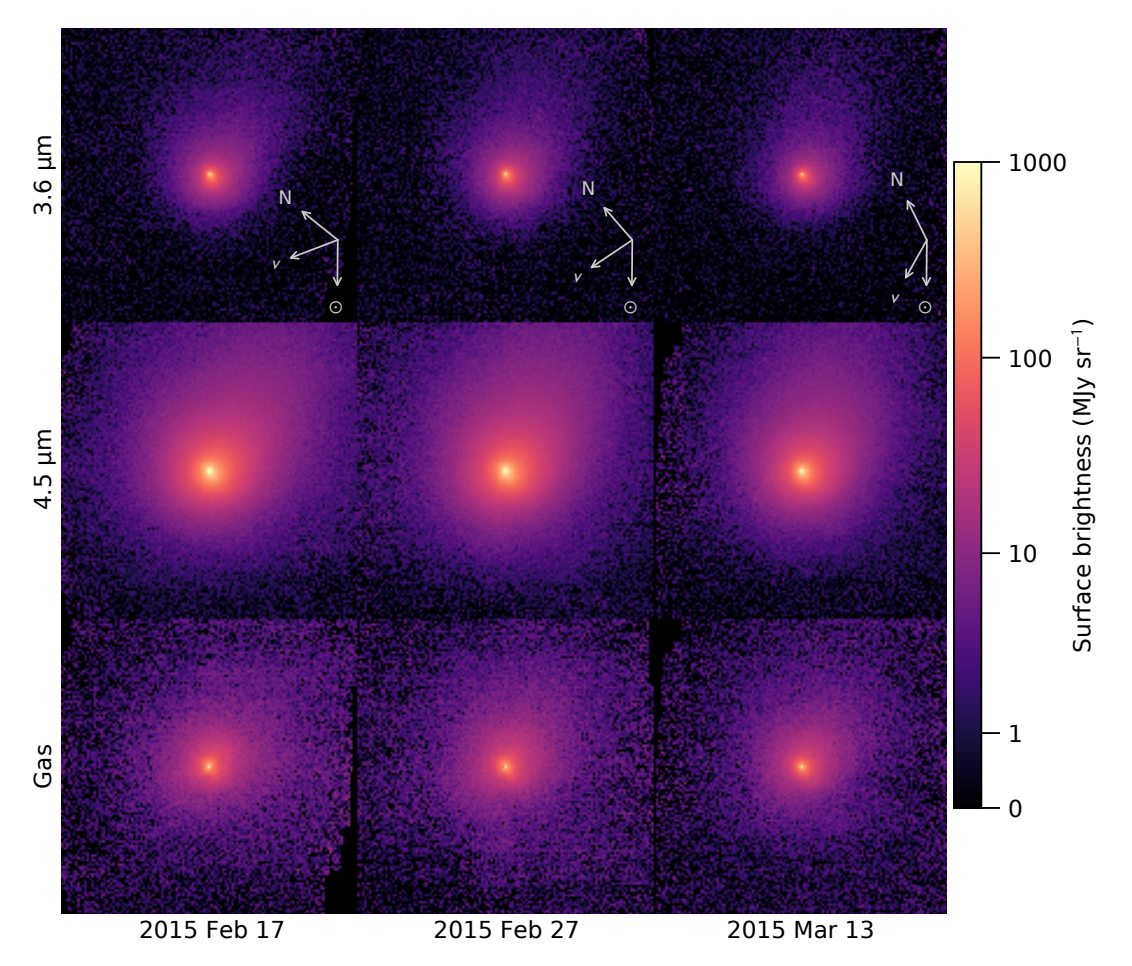


Figure 3. Spitzer IRAC images of comet C/2014 Q2 (Lovejoy). Top row: 3.6 μ m images. Center row: 4.5 μ m images. Bottom row: derived CO₂ gas maps. All images are displayed with an asinh color scale intended to show both the low-surface brightness instrumental background and the bright cometary core. Arrows indicate the projected Celestial north (N), Sun (\odot) and velocity (ν) vectors. Each sub-panel is $8.1 \times 8.1 \times 8.1$

image, then subtracting the two. Following previous work, we use a morphological technique to determine the scale factor, assuming the dust morphologies of the two images are the same (A. J. McKay et al. 2016). The gas coma is accounted for with a Haser model using the photodissociation rates for CO₂ from W. F. Huebner et al. (1992) and the same expansion speed as used for the water. Active sun photodissociation rates $(4.76 \times 10^{-6} \text{ s}^{-1} \text{ at 1 AU})$ produced a better fit to the coma than quiet sun rates, and were ultimately used for this work. The images are divided into a cylindrical grid with 30 radial steps (from 10 to 100 pixels) and 32 azimuthal

steps (from 0 to 360°). For each azimuthal step, the radial profiles of the 3.6 μ m image, 4.5 μ m image, and the model gas coma are calculated. With a least squares optimization technique, the scale factors for the dust and each azimuth bin of the gas coma are computed. A gas-only image is made and the coma brightness measured in a 24."4 (20 pix) radius aperture. The brightness is converted to production rate with a fluorescence *g*-factor of 2.69×10^{-3} photons s⁻¹ at 1 AU from the Sun (V. Debout et al. 2016), and the same Haser model as the morphological analysis. Uncertainties are based on IRAC pipeline uncertainty images. An additional 3% un-

certainty is assumed based on the absolute calibration of the instrument (W. T. Reach et al. 2005). Photometry, dust scale factors, and production rates are given in Table 3. The photometry is not color corrected in order to preserve the CO_2 irradiance.

For comet Lulin, a direct CO_2 measurement for comparison to our inferred value was made by T. Ootsubo et al. (2012). Their observations were obtained in the near-infrared using AKARI. The measurement of theirs that we reference in this work was obtained on UT 2009 February 5, around ten days before our own measurements. Observation geometries are provided in Table 3, with more details in T. Ootsubo et al. (2012).

3. RESULTS

We display a subset of our spectra for Lovejoy and Lulin with lines of best fit overplotted in Figures 4 and 5. We present initial oxygen line ratio measurements across multiple dates for each comet in Table 4. For photometric nights, we report $\rm H_2O$ production rates, from which we calculated a collisional quenching (CQ) factor. We divided the observed oxygen line ratio by the collisional quenching factor to obtain a new value for the oxygen line ratio that has been adjusted to account for collisional quenching. Table 4 shows our $\rm H_2O$ production rates, collisional quenching factors, and adjusted oxygen line ratios.

For non-photometric nights, absolute flux calibration was not possible, and therefore direct calculation of an H₂O production rate and CQ factor was not possible. For these nights, we adopted the CQ factor from the previous or following photometric night in order to calculate an adjusted oxygen line ratio. CQ factors were not adopted from nights more than a day apart, so we assume that any change between the H₂O production rate for the comet in this time frame would be negligible. For the spectrum obtained of Lovejoy on February 3 at an offset position (hereafter the "offset spectrum"), we elected not to calculate an H₂O production rate or CQ factor. For offset spectra, the production rate derived using the Haser model would not necessarily reflect the global production rate, and it is not required for our analysis. We discuss this spectrum more generally in terms of its unmodified oxygen line ratio in Section 4.1.

We calculate average oxygen line ratios of 0.031 ± 0.002 for the February 2-4 observations of Lovejoy and an average ratio of 0.041 ± 0.002 for the February 14-15 observations of Lulin. We use our calculated oxygen line ratios to infer CO_2 abundances via Equation 5 using the release rates from A. J. McKay et al. (2015) and A. Bhardwaj & S. Raghuram (2012) listed in Table 2. Table 5 shows CO_2 abundances for each comet inferred using the empirical release rates (A. J. McKay et al. 2015) and the theoretical release rates (A. Bhardwaj & S. Raghuram 2012). In the final

column, direct CO_2 measurements are shown from Spitzer (Lovejoy, this work) and AKARI (Lulin, T. Ootsubo et al. 2012), for comparison to the inferred abundances. For Lovejoy, we derive a direct CO_2 production rate based on a linear fit to the measured values extrapolated to February 3: $(4.47\pm0.25)\times10^{28}~{\rm s}^{-1}$. We divide our direct CO_2 production rate measurement from Spitzer by our calculated H_2O production rate from the [O I] 6300Å line flux to get the "direct" measurement of the $\frac{CO_2}{H_2O}$ ratio, since H_2O was not observed with Spitzer.

4. DISCUSSION

4.1. Lovejoy: Changes in [O I] ratio with heliocentric and cometocentric distance

Our average measured oxygen line ratio for Lovejoy in May is about 40% larger than the measured ratio in February, indicating that the oxygen line ratio increases with increasing heliocentric distance. This supports the well-established observation that H₂O sublimation falls off faster than CO₂ with heliocentric distance due to the higher volatility (lower sublimation temperature) of CO₂ (K. Meech & J. Svoren 2004; T. Ootsubo et al. 2012). The increase in Lovejoy's oxygen line ratio from February to May is indicative of a similar trend for this comet. Comparing the CO₂ abundance inferred from the February data to the abundance inferred in May, the abundance increased by about 50% using the empirical release rates and increased by almost 150% using the theoretical release rates. These results show that CO₂ may start to become a more important driver of activity even at heliocentric distances as small as 2 AU.

For the February 3 Lovejoy data, the "offset spectrum" produced a raw (i.e., unadjusted for collisional quenching) oxygen line ratio of 0.175 \pm 0.031, which is about a factor of 2 larger than the average raw oxygen line ratio of the other spectra obtained that same date that were centered on the comet's optocenter, which was 0.079 ± 0.002 . Even though collisional quenching is not accounted for yet in the raw oxygen line ratios, we can assert that the higher ratio for the offset spectrum is not due to any collisional quenching effects. This is because the amount of collisional quenching that occurs scales with density, and any offset position in the coma will be much less dense than the optocenter, meaning much less collisional quenching will occur at the offset position. The increased oxygen line ratio could be due to an anti-sunward asymmetry, but because species measured are neutral, one would not necessarily expect them to be enhanced along the tail. However, we cannot definitively rule out the the possibility that an anti-sunward jet is responsible for our higher measured oxygen line ratio at the offset coma

However, an increasing [O I] ratio with increasing cometocentric distance follows logically from what is known about

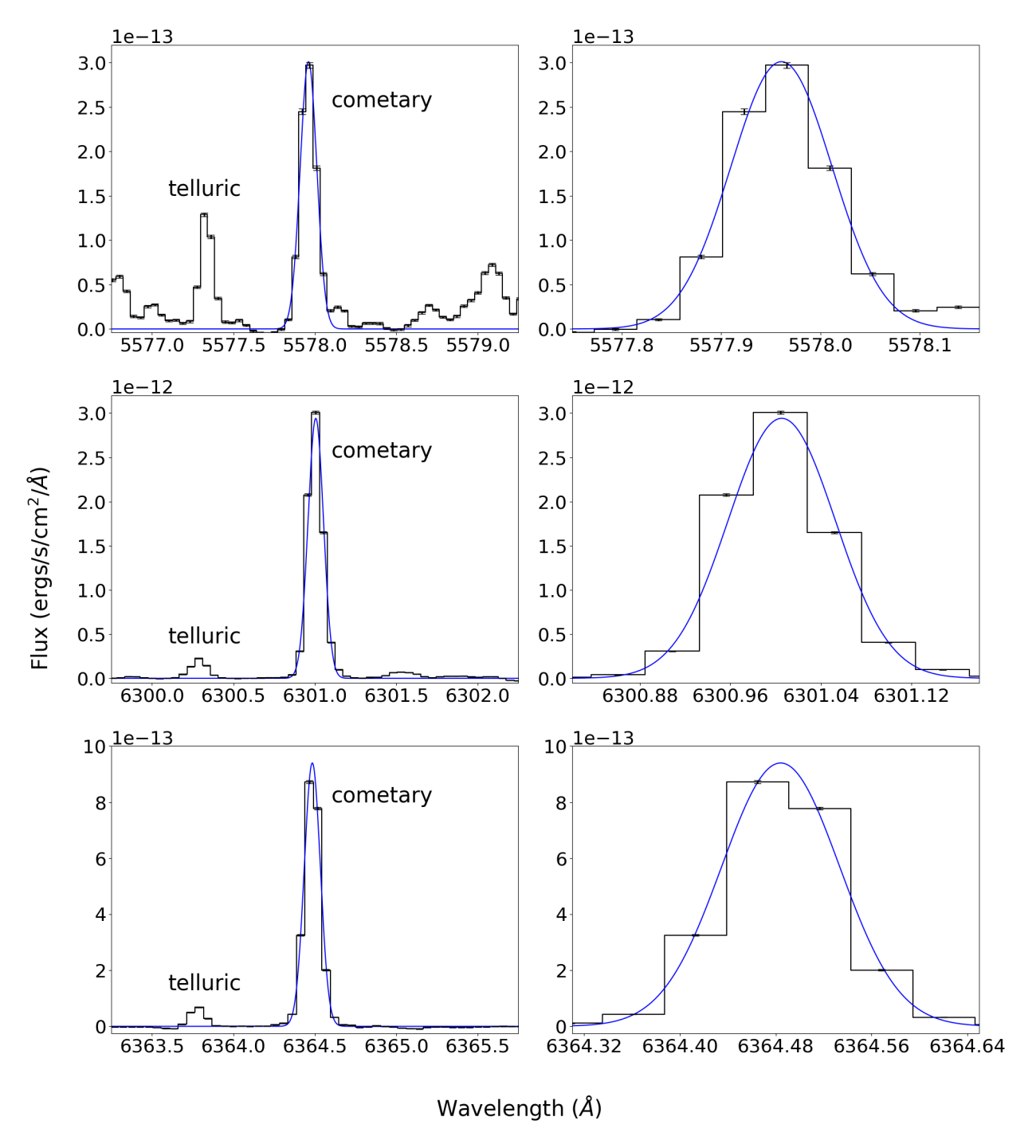


Figure 4. Regions of the spectra obtained of Lovejoy on UT 2015 February 3 that contain the forbidden oxygen lines at 5577Å (top row), 6300Å (middle row), and 6364Å (bottom row). Note that the cometary line appears redward of the telluric in all plots due to Doppler shifting caused by the comet's geocentric velocity. The data are represented by a histogram (black) with 1σ errorbars. The right column shows the cometary lines fitted with Gaussian curves (blue). The left column displays a zoomed-out view such that both the cometary and telluric lines are visible as well as the surrounding signal-to-noise. In the top left panel, the weaker features surrounding the two oxygen lines are due to emission from C_2 .

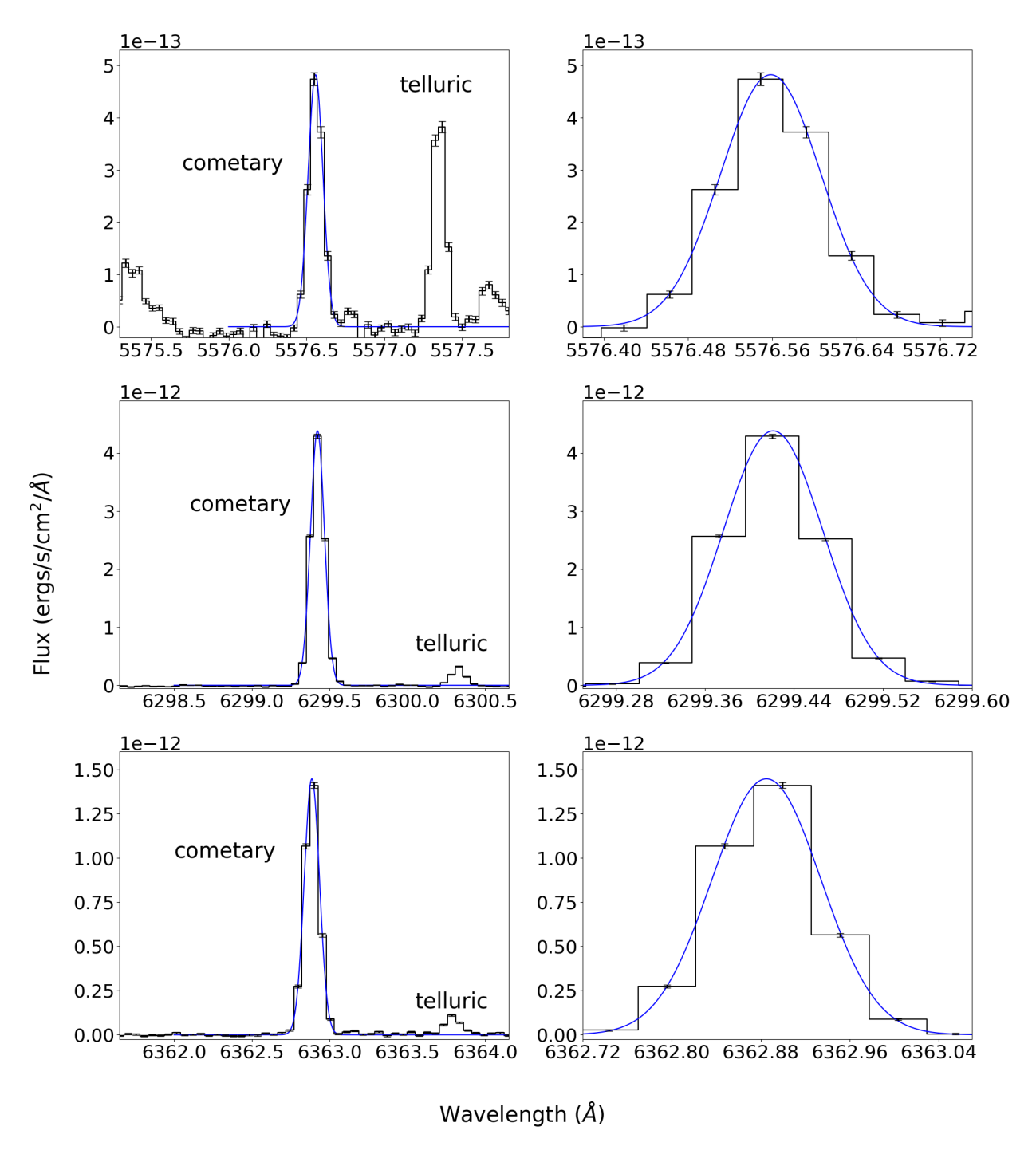


Figure 5. Regions of the spectra obtained of Lulin on UT 2009 February 14 that contain the forbidden oxygen lines at 5577Å (top row), 6300Å (middle row), and 6364Å (bottom row). Note that the cometary line appears blueward of the telluric in all plots due to Doppler shifting caused by the comet's geocentric velocity. The data are represented in the same ways described in Figure 4. In the top left panel, the weaker features surrounding the two oxygen lines are due to emission from C_2 .

Table 4. Oxygen line ratios and H_2O production rates. The sixth column contains the collisional quenching factor, which is derived from the H_2O production rate and is used to correct the $[O\ I]$ ratio. For non-photometric nights, calculating the H_2O production rate is not reliable, so instead the CQ factor from the previous or following night was used to get the adjusted oxygen line ratio.

Object	Date	r	[O I] line ratio	H ₂ O prod. rate	CQ factor	Adjusted [O I] ratio
	(UT)	(AU)		$(10^{29}s^{-1})$		
Lovejoy	2015 Feb 02	1.29	0.089 ± 0.006	•••	•••	0.033 ± 0.003
	2015 Feb 03	1.29	0.079 ± 0.005	6.57 ± 0.74	2.70 ± 0.10	0.029 ± 0.003
	2015 Feb 03 ^a	1.29	0.175 ± 0.031	•••	• • •	•••
	2015 Feb 04	1.29	0.085 ± 0.006	•••	• • •	0.031 ± 0.003
	2015 May 11	1.95	0.065 ± 0.004	1.19 ± 0.11	1.36 ± 0.02	0.048 ± 0.004
Lulin	2009 Feb 14	1.32	0.079 ± 0.004	•••	• • •	0.041 ± 0.003
	2009 Feb 15	1.33	0.080 ± 0.003	1.09 ± 0.11	1.94 ± 0.06	0.041 ± 0.002

^a Results for the "offset spectrum" obtained 100" tailward of the optocenter. We were not able to calculate a water production rate (and therefore a CO₂ abundance) for this spectrum because the Haser model only applies for water production at the center of the comet.

Table 5. CO₂ abundances inferred using the adjusted oxygen line ratios from Table 4. The abbreviation "emp." refers to the empirical release rates from A. J. McKay et al. (2015), and "th." refers to the theoretical release rates from A. Bhardwaj & S. Raghuram (2012). The two inferred CO₂ abundances are listed next to the directly measured CO₂ abundances ("dir.") from Spitzer (this work) and AKARI (T. Ootsubo et al. 2012).

Object	Date	$\frac{CO_2}{H_2O}$ emp.	$\frac{CO_2}{H_2O}$ th.	$\frac{CO_2}{H_2O}$ dir.
	(UT)	(%)	(%)	(%)
Lovejoy	2015 Feb 2-4	7.2 ± 0.6	0.5 ± 0.3	7.4 ± 0.4^{a}
	2015 May 11	12.7 ± 1.3	3.0 ± 0.6	
Lulin	2009 Feb 14-15	10.4 ± 0.7	1.9 ± 0.3	11.9 ± 1.7^{b}

^aAbundance calculated using inferred CO₂ production rate for February 3 extrapolated from line fit to direct measurements obtained by Spitzer over three dates in 2015 February-March (see Section 2.2).

the scale lengths for photodissociation of H₂O vs. CO₂. In cometary comae, H₂O has a scale length of about 80,000 km, while CO₂ has a scale length of about 500,000 km due to the longer lifetime of CO₂ in the coma (D. Bockelee-Morvan & J. Crovisier 1989; W. F. Huebner et al. 1992). The spectrum's offset distance of 100" is equivalent to a linear distance of roughly 60,000 km, which is comparable to the H₂O scale length, but an order of magnitude less than the CO₂ scale length. It is reasonable to expect that with increasing distance from the center of the comet, H₂O will be lost preferentially over CO₂, and thus CO₂ will play a larger role in supplying the [O I] population in the outer coma, increasing the oxygen line ratio for offset spectra such as in this work. Indeed, some analysis of this phenomenon has been conducted in other works (e.g., T. Nelson & A. Cochran 2021). However, more study is still needed to confirm this potential trend of increasing [O I] ratio with cometocentric distance. In future work, more spatially resolved observations of the oxygen coma could shed more light on the dependence of the oxygen line ratio on cometocentric distance.

4.2. Water production rates
4.2.1. Lovejoy

We compare our calculated H_2O production rate for Lovejoy on 2015 February 3 to other works that have reported production rates from observations obtained very near to our own. N. Biver et al. (2015) took observations of water with IRAM from January 30 to February 3 and reported an H_2O production rate of $(7.5 \pm 0.3) \times 10^{29} \ s^{-1}$. SOHO/SWAN observations on February 3 from M. Combi et al. (2018) resulted in a production rate of $(5.9140 \pm 0.6805) \times 10^{29} \ s^{-1}$. NIRSPEC observations on February 3 from N. Dello Russo et al. (2022) resulted in a production rate of $\sim (5-8) \times 10^{29} \ s^{-1}$. NIRSPEC observations on February 4 and 5 by L. Paganini et al. (2017) resulted in a production rate of $(5.9 \pm 0.13) \times 10^{29} \ s^{-1}$. All of these measurements agree with our own production rate of $(6.57 \pm 0.74) \times 10^{29} \ s^{-1}$ within uncertainty.

Other measurements from the literature do not agree with our water production value as closely. Near-infrared observations obtained by S. Faggi et al. (2016) from January 30 - February 2 produced a production rate of (4.88 \pm 0.22) \times 10²⁹ s^{-1} . P. D. Feldman et al. (2018) reported a production rate of (4.5 \pm 0.9) \times 10²⁹ s^{-1} from HST observations ob-

b Direct measurement obtained by AKARI on UT 2009 February 5. Cited from T. Ootsubo et al. (2012).

tained on February 2. N. Biver et al. (2016) reported a production rate of $(8.7 \pm 0.7) \times 10^{29}~s^{-1}$ using the *Odin* submillimeter space observatory from January 29 - February 3. None of these measurements agree with our production rate within uncertainty, but the differences are all $\leq 2.2\sigma$. The discrepancy is reduced further after considering additional uncertainty from rotational variation. The *Odin* observations indicated significant variability in the water production rate across the observation date range, which overlaps very closely over our own range. They showed that the variability of the water production rate over this date range fit approximately to a sine wave with an amplitude of $\pm 20\%$. Taking this variation into account as additional uncertainty, all three discrepant values above agree with our measurement.

We also compare our calculated H₂O production rate for Lovejoy on May 11 to an additional production rate measurement from M. Combi et al. (2018) on May 11. They reported an H₂O production rate of $(2.1820 \pm 0.0087) \times 10^{29} \text{ s}^{-1}$, which is about a factor of two larger than our measurement of $(1.19 \pm 0.11) \times 10^{29} \, s^{-1}$. However, some previous works (e.g., A. J. McKay et al. 2015) have found SWAN to give systematically high water production rates, likely because it detects production from icy grains in the outer coma, which would not be included in our calculations of production in the inner coma. The agreement between our February values could be related to the shorter sublimation lifetimes of the icy grains at smaller heliocentric distances, which could result in the grains mostly sublimating within our observation aperture, eliminating the discrepancy between our smaller field observations and the wider field of view of SWAN. However, it is important to note that while these effects could explain the discrepancy in our water production rates, this would not cause any change in the [O I] ratio or inferred CO₂ abundance, for the purposes of this work.

4.2.2. Lulin

We compare our calculated H₂O production rate for Lulin on 2009 February 15 to other works that have reported production rates for Lulin near this date. NIRSPEC observations from January 30 - February 1 by E. L. Gibb et al. (2012) reported production rates between $(1.13 \pm 0.02) \times 10^{29} \, s^{-1}$ and $(2.68 \pm 0.11) \times 10^{29} \, s^{-1}$, which agrees with our measurement of $(1.09 \pm 0.11) \times 10^{29} \, s^{-1}$ within uncertainty. However, other works reported production rates that do not agree with our measurement. Swift observations obtained by D. Bodewits et al. (2010) on January 28 yielded production rates between $\sim (6.7-7.9 \pm 0.7) \times 10^{29} \text{ s}^{-1}$, which is about 6 times larger than our measurement. AKARI observations from February 5 by T. Ootsubo et al. (2012) resulted in a production rate of $(4.091 \pm 0.409) \times 10^{28} \text{ s}^{-1}$, and narrowband photometry obtained on February 26 by A. N. Bair et al. (2018) resulted in a production rate of $(6.0 \pm 0.3) \times 10^{28} \ s^{-1}$. These are each about a factor of 2 lower than our measurement.

Water production in Lulin around these dates is clearly complex, given these several discrepant values found by various sources. E. L. Gibb et al. (2012) found that their measured water production rate fluctuated significantly even over a timescale of hours, and began steadily increasing the last date of their observations (February 1). They suggested that this variability could be due to a rotating jet morphology. Additionally, M. R. Combi et al. (2019) predicted a water production rate that decreases with heliocentric distance postperihelion according to the power law:

$$Q = Q_1 r^{-p} \tag{7}$$

where Q represents the water production rate, Q_1 represents the production rate at 1 AU, r represents heliocentric distance, and p represents the power-law exponent. For measurements of Lulin between 2009 January 10 and 2009 April 21, M. R. Combi et al. (2019) reported $Q_1 = 1.78 \times 10^{29}$ and $p = -1.7 \pm 0.1$. We plot this relation over each of the water production rates for Lulin discussed here in Figure 6. The data seem to generally follow the shape of the curve, with the production rate from D. Bodewits et al. (2010) as a clear outlier. The production rate from T. Ootsubo et al. (2012) also appears to be an underestimate compared to the overall fit and an outlier to the overall trend of decreasing production rate with increasing heliocentric distance. An underestimate for water production measured from infrared observations could be due to optical depth effects that were unaccounted for, which may become significant at production rates on the order of $10^{29} \, s^{-1}$ such as these. If the production rate from T. Ootsubo et al. (2012) was indeed an underestimate due to optical depth effects, their calculated CO₂ abundance would have also been affected. We discuss this further in Section 4.3.

Despite some discrepancy between our H_2O production rate for Lulin and values in the literature, our production rate for Lovejoy agrees well with most other values. Additionally, calculating H_2O production rates from the 6300Å line flux is shown to be a generally reliable method in other works (J. P. Morgenthaler et al. 2001, 2007; U. Fink 2009; A. J. McKay et al. 2018, 2021).

4.3. Inferred CO₂ abundances

Of the two calculated $\frac{CO_2}{H_2O}$ ratios for Lovejoy, the ratio inferred using the empirical release rates from A. J. McKay et al. (2015) reproduces the direct measurement made by Spitzer within uncertainty, while the ratio inferred using the theoretical release rates from A. Bhardwaj & S. Raghuram (2012) is approximately an order of magnitude lower than the direct measurement. The empirical release rates from A. J. McKay et al. (2015) were calculated using data from

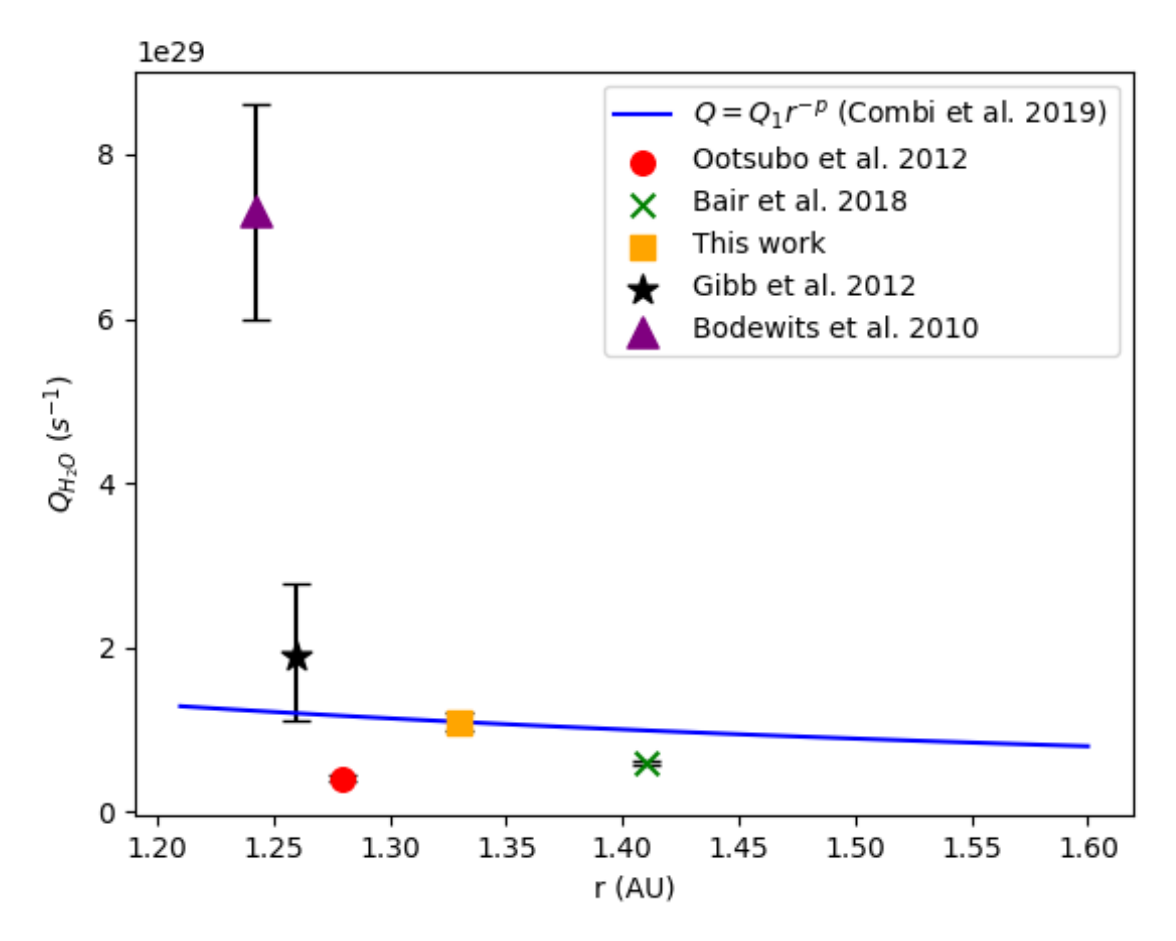


Figure 6. Water production rates for Lulin from the literature, fitted to the power law prediction by M. R. Combi et al. (2019) for the relationship between water production rate and heliocentric distance post-perihelion. The data generally follow the curve, with the production rate from D. Bodewits et al. (2010) as a clear outlier, and the production rate from T. Ootsubo et al. (2012) a more subtle outlier. The uncertainty on the production rate from A. N. Bair et al. (2018) represents the standard deviation of their measurements. For the production rates from T. Ootsubo et al. (2012), A. N. Bair et al. (2018), and this work, the error bars are smaller than the size of the marker on the graph.

a comet observed near solar maximum. Lovejoy was also observed near solar maximum in this work, and the empirical release rates were the most accurate at inferring a CO_2 abundance for Lovejoy using these observations. However, the empirical release rates were also the most accurate at inferring a CO_2 abundance for Lulin, which was observed near solar minimum.

This could suggest that solar activity plays little role and the discrepancy between the two sets of release rates is due to some other unknown factor. However, for infrared observations such as those from T. Ootsubo et al. (2012), the water production rate was determined from lines that could become optically thick for production rates on the order of $10^{29} \ s^{-1}$ (such as theirs and those reported by other works, cited in Section 4.2.2). If the coma was optically thick at the infrared observation wavelengths, the water production rate from T. Ootsubo et al. (2012) could have been an underestimate. However, their CO₂ production rate was likely small

enough to remain optically thin (on the order of $10^{27} s^{-1}$), and was likely a more accurate estimate of the true production. Therefore, the $\frac{CO_2}{H_2O}$ ratio reported by T. Ootsubo et al. (2012) could be an overestimate due to the H₂O production rate in the denominator being an underestimate. Ootsubo et al. addressed this possibility in an earlier work (T. Ootsubo et al. 2010) by measuring the water production rate via observations offset from the comet's optocenter. However, these measurements were taken about 6 weeks after our own, compared to the measurements from T. Ootsubo et al. (2012) that are only 10 days before ours. Additionally, optocenterderived vs. offset-derived production rate ratios may not be directly comparable due to asymmetries in the coma. Our measurements were taken centered on the optocenter, so our inferred $\frac{CO_2}{H_2O}$ ratio may not be comparable to the ratio reported in T. Ootsubo et al. (2010). For these reasons, comparison to the measurements from T. Ootsubo et al. (2012) is likely still more relevant for our purposes. However, it is also worth considering that if the $\frac{CO_2}{H_2O}$ ratio varies with rotational phase, that could complicate the interpretation of comparison with either AKARI measurement.

Because our water production rate agrees better with the other values reported in the literature and with the power law relationship from M. R. Combi et al. (2019), we recalculated the $\frac{CO_2}{H_2O}$ reported in T. Ootsubo et al. (2012) by dividing their CO₂ production rate by our water production rate. Using this updated ratio of 4.4% \pm 0.5%, the inferred abundance using the empirical release rates is no longer in agreement with the direct measurement. The abundance inferred using the theoretical release rates also does not accurately reproduce this updated ratio. However, several works using these release rates from A. Bhardwaj & S. Raghuram (2012) report that they fail to reproduce direct measurements (A. J. McKay et al. 2013, 2015, 2016). Therefore, it is not surprising that using this set of release rates did not accurately reproduce the direct measurements for either of these comets. In contrast, the empirical release rates reproduced the direct measurement for Lovejoy, but not for Lulin (using the updated ratio from T. Ootsubo et al. (2012)). This could be explained by differences in solar activity assumption between the empirical release rates and the actual observations.

4.4. Solar activity effects

Because oxygen atom release into the coma is caused by photodissociation via UV photons, changes in the intensity of the sun's UV output could be reflected in a changing oxygen atom release rate. Indeed, previous work has also shown that solar activity affects the scale lengths of species such as water (A. L. Cochran & D. G. Schleicher (1993) and references therein). We retrieved the solar spectra on the days of our observations of both Lovejoy and Lulin from the LASP Interactive Solar Irradiance Datacenter (LISIRD) database (Laboratory for Atmospheric and Space Physics 2005) in order to examine any differences between them. The top panel of Figure 7 shows the total solar spectral irradiance plotted as a function of wavelength on two dates corresponding to our observations of Lovejoy (2015 February 3) and Lulin (2009 February 15). The bottom panel shows the ratio of the solar quiet spectrum to the solar active spectrum. The spectrum nearer to solar minimum (blue) maintains a consistently lower irradiance than the spectrum nearer to solar maximum. The bottom panel shows that the difference between the two spectra is more drastic at shorter wavelengths. In the top panel, this is especially clear at the Lyman-alpha line at 121.6 nm, of which a zoomed-in view is shown. Because the Lyman-alpha line is an important contributor to photodissociation rates, a difference in solar irradiance at this line due to the solar cycle could affect the photochemistry of [O I] release, perhaps even enough to affect the inferred $\frac{CO_2}{H_2O}$ ratio from the oxygen line ratios. If so, it would be necessary to

consider the solar cycle when deciding what release rates to use to calculate the oxygen line ratio. However, more work is needed to determine if the discrepancies we see in this work are consistent with what is expected from a changing UV spectrum. This would likely require more detailed modeling that is beyond the scope of this work.

5. CONCLUSION

We present analysis of the forbidden oxygen lines at 5577, 6300, and 6364Å for comets C/2014 Q2 (Lovejoy) and C/2007 N3 (Lulin). We calculate oxygen line ratios for each observation date and use them to calculate inferred CO₂ abundances, which we compare with direct measurements obtained by spacecraft near our observation dates. Our results suggest that the oxygen line ratio likely increases both with cometocentric and heliocentric distance. Additionally, we report water production rates for both comets that are consistent with most other values reported the literature when rotational variability and other effects such as optical depth are taken into consideration. When comparing CO₂ abundances, we find that using the empirical [O I] release rates from A. J. McKay et al. (2015) reproduces the direct CO₂ measurement for Lovejoy. When avoiding optical depth effects on water production in the coma at infrared wavelengths, we find that the empirical release rates do not reproduce the direct CO₂ measurement for Lulin. We suggest that this discrepancy could be due to differences in solar activity.

Because our inferred CO₂ abundance for Lovejoy using the empirical release rates accurately reproduced the direct measurement obtained by spacecraft, our results add to the growing body of work supporting the validity of the oxygen line ratio as a proxy for direct CO₂ measurement. However, the dependence of these inferred CO2 abundances on the choice of release rates and the possible correlation between the release rates' accuracy and the level of solar activity at the time of observation/release rate calculation suggests the factor of solar activity needs to be incorporated into the oxygen line ratio method. Because of the strong possibility that the solar cycle plays a significant role in the photochemistry of [O I] release, using the oxygen line ratio as a proxy for direct CO₂ measurement will not be a fully reliable method until this relationship is understood and quantified. Future work should examine a more robust sample of comets observed at varying levels of solar activity to confirm and characterize the relationship between the solar cycle and release rate accuracy. Once this relationship's effect on coma photochemistry is more fully understood, the oxygen line ratio method may become an important strategy for determining CO₂ abundances, increasing our knowledge about this important molecule's behavior in cometary comae.

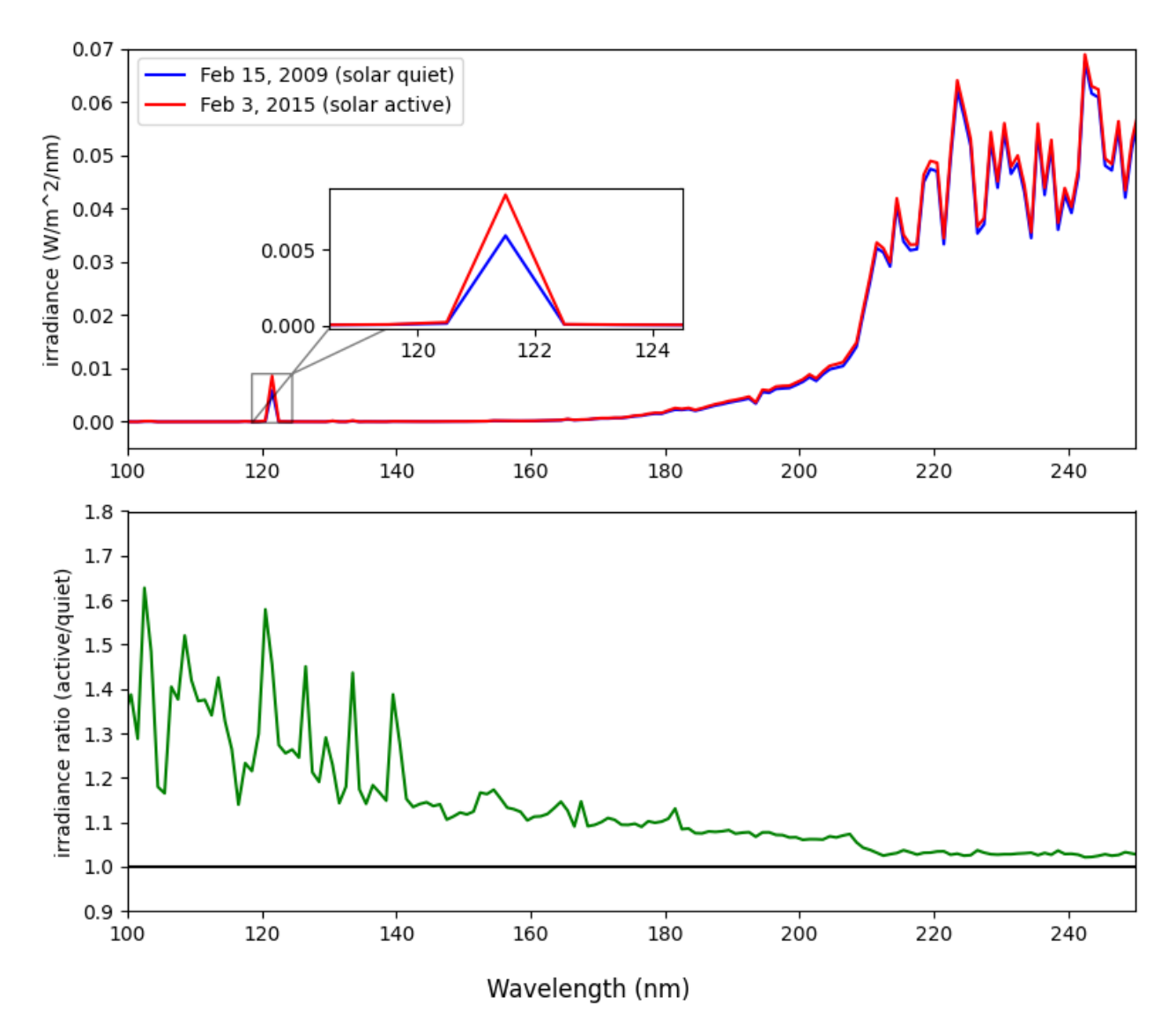


Figure 7. Top panel: Total solar spectral irradiance for two dates plotted as a function of wavelength. The two dates plotted correspond to two of our observation dates, one each for Lovejoy and Lulin. The bottom panel plots the ratio between the two spectra (green), with the straight black line showing a ratio equal to one for easier visual comparison. The solar quiet spectrum is shown to have a consistently lower irradiance, such that the ratio is always greater than one. However, the difference is more pronounced at shorter wavelengths, particularly at the Lyman-alpha line, which is shown in a zoomed-in box in the top panel. Data retrieved from the LASP Interactive Solar Irradiance Datacenter (LISIRD) database (Laboratory for Atmospheric and Space Physics 2005).

ACKNOWLEDGEMENTS

This work was supported by the NASA Solar System Workings Program through grant 80NSSC20K0140 and by NASA through an award issued by JPL/Caltech to Appalachian State University. This paper includes data obtained at the McDonald Observatory of The University of Texas at Austin. This paper also contains observations made with the Spitzer Space Telescope, which was operated by the Jet Propulsion Laboratory, California Institute of Technology under a contract with NASA. Support for the work with Spitzer was provided by NASA through an award issued by JPL/Caltech. We acknowledge the JPL Horizons System, which was used during

observations to generate ephemerides for nonsidereal tracking of the comets. Additionally, we acknowledge the SIM-BAD database, which was used for the selection of standard stars.

Facility: Spitzer (IRAC), IRSA (Spitzer Heritage Archive)

Facility: McDonald Observatory (2.7m Tull Coudé Spectrograph)

Software: Scipy (P. Virtanen et al. 2020), Astropy (Astropy Collaboration et al. 2013, 2018, 2022), sbpy (M. Mommert et al. 2019), Pyspeckit (A. Ginsburg et al. 2022)

REFERENCES

- Astropy Collaboration, Robitaille, T. P., Tollerud, E. J., et al. 2013, Astropy: A community Python package for astronomy, A&A, 558, A33, doi: 10.1051/0004-6361/201322068
- Astropy Collaboration, Price-Whelan, A. M., Sipőcz, B. M., et al. 2018, The Astropy Project: Building an Open-science Project and Status of the v2.0 Core Package, AJ, 156, 123, doi: 10.3847/1538-3881/aabc4f
- Astropy Collaboration, Price-Whelan, A. M., Lim, P. L., et al. 2022, The Astropy Project: Sustaining and Growing a Community-oriented Open-source Project and the Latest Major Release (v5.0) of the Core Package, ApJ, 935, 167, doi: 10.3847/1538-4357/ac7c74
- Bair, A. N., Schleicher, D. G., & Knight, M. M. 2018, Coma Morphology, Numerical Modeling, and Production Rates for Comet C/Lulin (2007 N3), The Astronomical Journal, 156, 159, doi: 10.3847/1538-3881/aad549
- Bhardwaj, A., & Raghuram, S. 2012, A COUPLED CHEMISTRY-EMISSION MODEL FOR ATOMIC OXYGEN GREEN AND RED-DOUBLET EMISSIONS IN THE COMET C/1996 B2 HYAKUTAKE, The Astrophysical Journal, 748, 13, doi: 10.1088/0004-637x/748/1/13
- Biver, N., Bockelée-Morvan, D., Moreno, R., et al. 2015, Ethyl alcohol and sugar in comet C/2014 Q2 (Lovejoy), Science Advances, 1, doi: 10.1126/sciadv.1500863
- Biver, N., Moreno, R., Bockelée-Morvan, D., et al. 2016, Isotopic ratios of H, C, N, O, and S in comets C/2012 F6 (Lemmon) and C/2014 Q2 (Lovejoy), Astronomy & Astrophysics, 589, A78, doi: 10.1051/0004-6361/201528041
- Bockelee-Morvan, D., & Crovisier, J. 1989, The nature of the 2.8-micron emission feature in cometary spectra, A&A, 216, 278
- Bodewits, D., Villanueva, G. L., Mumma, M. J., et al. 2010, SWIFT-UVOT GRISM SPECTROSCOPY OF COMETS: A FIRST APPLICATION TO C/2007 N3 (LULIN), The Astronomical Journal, 141, 12, doi: 10.1088/0004-6256/141/1/12
- Budzien, S. A., Festou, M. C., & Feldman, P. D. 1994, Solar Flux Variability and the Lifetimes of Cometary H ₂O and OH, Icarus, 107, 164, doi: 10.1006/icar.1994.1014
- Cochran, A. 2001, Observations of O (1S) and O (1D) in Spectra of C/1999 S4 (LINEAR), Icarus, 154, 381, doi: 10.1006/icar.2001.6718
- Cochran, A. L. 2008, Atomic oxygen in the comae of comets, Icarus, 198, 181, doi: 10.1016/j.icarus.2008.06.007

- Cochran, A. L., & Schleicher, D. G. 1993, Observational Constraints on the Lifetime of Cometary H ₂O, Icarus, 105, 235, doi: 10.1006/icar.1993.1121
- Combi, M., Mäkinen, T., Bertaux, J.-L., et al. 2018, Water production activity of nine long-period comets from SOHO/SWAN observations of hydrogen Lyman-alpha: 2013–2016, Icarus, 300, 33–46, doi: 10.1016/j.icarus.2017.08.035
- Combi, M. R., Mäkinen, T. T., Bertaux, J.-L., Quémerais, E., & Ferron, S. 2019, A survey of water production in 61 comets from SOHO/SWAN observations of hydrogen Lyman-alpha: Twenty-one years 1996-2016, Icarus, 317, 610, doi: 10.1016/j.icarus.2018.08.031
- Debout, V., Bockelée-Morvan, D., & Zakharov, V. 2016, A radiative transfer model to treat infrared molecular excitation in cometary atmospheres, Icarus, 265, 110, doi: 10.1016/j.icarus.2015.10.013
- Decock, A., Jehin, E., Hutsemékers, D., & Manfroid, J. 2013, Forbidden oxygen lines in comets at various heliocentric distances, Astronomy & Astrophysics, 555, A34, doi: 10.1051/0004-6361/201220414
- Decock, A., Jehin, E., Rousselot, P., et al. 2014, Forbidden oxygen lines at various nucleocentric distances in comets, Astronomy & Astrophysics, 573, A1, doi: 10.1051/0004-6361/201424403
- Dello Russo, N., Vervack, R. J., Kawakita, H., et al. 2022, Volatile Abundances, Extended Coma Sources, and Nucleus Ice Associations in Comet C/2014 Q2 (Lovejoy), The Planetary Science Journal, 3, 6, doi: 10.3847/psj/ac323c
- Delsemme, A. 1980, Photodissociation of CO₂ into CO + O(¹D), The spectra of simple molecules in the laboratory and in astrophysics.
 - articles.adsabs.harvard.edu/pdf/1980LIACo..21..515D
- Faggi, S., Villanueva, G. L., Mumma, M. J., et al. 2016, DETAILED ANALYSIS OF NEAR-IR WATER (H2O) EMISSION IN COMET C/2014 Q2 (LOVEJOY) WITH THE GIANO/TNG SPECTROGRAPH, The Astrophysical Journal, 830, 157, doi: 10.3847/0004-637x/830/2/157
- Fazio, G. G., Hora, J. L., Allen, L. E., et al. 2004, The Infrared Array Camera (IRAC) for the Spitzer Space Telescope, ApJS, 154, 10, doi: 10.1086/422843

- Feldman, P. D., Weaver, H. A., A'Hearn, M. F., Combi, M. R., & Russo, N. D. 2018, Far-ultraviolet Spectroscopy of Recent Comets with the Cosmic Origins Spectrograph on the Hubble Space Telescope, The Astronomical Journal, 155, 193, doi: 10.3847/1538-3881/aab78a
- Festou, M. C., & Feldman, P. D. 1981, The Forbidden Oxygen Lines in Comets, Astronomy and Astrophysics. https://articles.adsabs.harvard.edu/pdf/1981A%26A...103..154F
- Fink, U. 2009, A taxonomic survey of comet composition 1985-2004 using CCD spectroscopy, Icarus, 201, 311, doi: 10.1016/j.icarus.2008.12.044
- Gibb, E. L., Bonev, B. P., Villanueva, G., et al. 2012, CHEMICAL COMPOSITION OF COMET C/2007 N3 (LULIN): ANOTHER "ATYPICAL" COMET, The Astrophysical Journal, 750, 102, doi: 10.1088/0004-637x/750/2/102
- Ginsburg, A., Sokolov, V., de Val-Borro, M., et al. 2022, Pyspeckit: A Spectroscopic Analysis and Plotting Package, The Astronomical Journal, 163, 291, doi: 10.3847/1538-3881/ac695a
- Hall, K., McKay, A., Kelley, M., et al. 2021, in AAS/Division for Planetary Sciences Meeting Abstracts, Vol. 53, AAS/Division for Planetary Sciences Meeting Abstracts #53, 210.07
- Haser, L. 1957, Distribution d'intensité dans la tête d'une comète, Bulletins de l'Académie Royale de Belgique, 43, 740
- Huebner, W. F., Keady, J. J., & Lyon, S. P. 1992, Solar photo rates for planetary atmospheres and atmospheric pollutants, Astrophysics and Space Science, 195, 1–294, doi: 10.1007/bf00644558
- IRSA. 2022, Spitzer Heritage Archive (SHA), IPAC, doi: 10.26131/IRSA543
- Kelley, M. S., Bodewits, D., Feaga, L. M., et al. 2017, in AAS/Division for Planetary Sciences Meeting Abstracts,Vol. 49, AAS/Division for Planetary Sciences Meeting Abstracts #49, 414.15
- Laboratory for Atmospheric and Space Physics. 2005, LASP Interactive Solar Irradiance Datacenter, Laboratory for Atmospheric and Space Physics, doi: 10.25980/L27Z-XD34
- Laine, S., ed. 2010, IRAC Instrument Handbook (Pasadena: Spitzer Science Center).
 - http://ssc.spitzer.caltech.edu/irac/iracinstrumenthandbook/
- Makovoz, D., & Khan, I. 2005, in Astronomical Society of the Pacific Conference Series, Vol. 347, Astronomical Data Analysis Software and Systems XIV, ed. P. Shopbell, M. Britton, & R. Ebert, 81
- McKay, A., Kelley, M., Cochran, A., DiSanti, M., & Bauer, J. 2020, in AAS/Division for Planetary Sciences Meeting Abstracts, Vol. 52, AAS/Division for Planetary Sciences Meeting Abstracts #52, 108.02

- McKay, A. J., Chanover, N. J., DiSanti, M. A., et al. 2014, Rotational variation of daughter species production rates in Comet 103P/Hartley: Implications for the progeny of daughter species and the degree of chemical heterogeneity, Icarus, 231, 193, doi: 10.1016/j.icarus.2013.11.029
- McKay, A. J., Chanover, N. J., Morgenthaler, J. P., et al. 2012, Forbidden oxygen lines in Comets C/2006 W3 Christensen and C/2007 Q3 Siding Spring at large heliocentric distance: Implications for the sublimation of volatile ices, Icarus, 220, 277, doi: 10.1016/j.icarus.2012.04.030
- McKay, A. J., Chanover, N. J., Morgenthaler, J. P., et al. 2013, Observations of the forbidden oxygen lines in DIXI target Comet 103P/Hartley, Icarus, 222, 684, doi: 10.1016/j.icarus.2012.06.020
- McKay, A. J., Cochran, A. L., DiSanti, M. A., et al. 2018, Evolution of H₂O production in comet C/2012 S1 (ISON) as inferred from forbidden oxygen and OH emission, Icarus, 309, 1, doi: 10.1016/j.icarus.2018.02.024
- McKay, A. J., Kelley, M. S., Cochran, A. L., et al. 2016, The CO 2 abundance in Comets C/2012 K1 (PanSTARRS), C/2012 K5 (LINEAR), and 290P/Jäger as measured with Spitzer, Icarus, 266, 249, doi: 10.1016/j.icarus.2015.11.004
- McKay, A. J., Cochran, A. L., DiSanti, M. A., et al. 2015, Evolution of H2O, CO, and CO2 production in Comet C/2009 P1 Garradd during the 2011–2012 apparition, Icarus, 250, 504, doi: 10.1016/j.icarus.2014.12.023
- McKay, A. J., DiSanti, M. A., Cochran, A. L., et al. 2021, Quantifying the Hypervolatile Abundances in Jupiter-family Comet 46P/Wirtanen, PSJ, 2, 21, doi: 10.3847/PSJ/abd71d
- Meech, K., & Svoren, J. 2004, Using cometary activity to trace the physical and chemical evolution of cometary nuclei, Comets II
- Mommert, M., Kelley, M., de Val-Borro, M., et al. 2019, sbpy: A Python module for small-body planetary astronomy, The Journal of Open Source Software, 4, 1426, doi: 10.21105/joss.01426
- Morgenthaler, J. P., Harris, W. M., & Combi, M. R. 2007, Large Aperture O I 6300 Å Observations of Comet Hyakutake: Implications for the Photochemistry of OH and O I Production in Comet Hale-Bopp, ApJ, 657, 1162, doi: 10.1086/511062
- Morgenthaler, J. P., Harris, W. M., Scherb, F., et al. 2001, Large-Aperture [O I] 6300 Å Photometry of Comet Hale-Bopp: Implications for the Photochemistry of OH, ApJ, 563, 451, doi: 10.1086/323773
- Nelson, T., & Cochran, A. 2021, in AAS/Division for Planetary Sciences Meeting Abstracts, Vol. 53, AAS/Division for Planetary Sciences Meeting Abstracts #53, 102.03
- Ootsubo, T., Usui, F., Kawakita, H., et al. 2010, DETECTION OF PARENT H2O AND CO2MOLECULES IN THE 2.5–5 μm SPECTRUM OF COMET C/2007 N3 (LULIN) OBSERVED WITHAKARI, The Astrophysical Journal, 717, L66–L70, doi: 10.1088/2041-8205/717/1/166

- Ootsubo, T., Kawakita, H., Hamada, S., et al. 2012, AKARI NEAR-INFRARED SPECTROSCOPIC SURVEY FOR CO2IN 18 COMETS, The Astrophysical Journal, 752, 15, doi: 10.1088/0004-637x/752/1/15
- Paganini, L., Mumma, M. J., Gibb, E. L., & Villanueva, G. L. 2017, Ground-based Detection of Deuterated Water in Comet C/2014 Q2 (Lovejoy) at IR Wavelengths, The Astrophysical Journal Letters, 836, L25, doi: 10.3847/2041-8213/aa5cb3
- Raghuram, S., & Bhardwaj, A. 2014, Photochemistry of atomic oxygen green and red-doublet emissions in comets at larger heliocentric distances, Astronomy & Astrophysics, 566, A134, doi: 10.1051/0004-6361/201321921
- Raghuram, S., Hutsemékers, D., Opitom, C., et al. 2020, Forbidden atomic carbon, nitrogen, and oxygen emission lines in the water-poor comet C/2016 R2 (Pan-STARRS), Astronomy & Astrophysics, 635, A108, doi: 10.1051/0004-6361/201936713
- Reach, W. T., Kelley, M. S., & Vaubaillon, J. 2013, Survey of cometary CO₂, CO, and particulate emissions using the Spitzer Space Telescope, Icarus, 226, 777, doi: 10.1016/j.icarus.2013.06.011
- Reach, W. T., Megeath, S. T., Cohen, M., et al. 2005, Absolute Calibration of the Infrared Array Camera on the Spitzer Space Telescope, PASP, 117, 978, doi: 10.1086/432670
- Sharpee, B. D., & Slanger, T. G. 2006, $O(^1D_2 ^3P_{2,1,0})$ 630.0, 636.4, and 639.2 nm Forbidden Emission Line Intensity Ratios Measured in the Terrestrial Nightglow, The Journal of Physical Chemistry A, 110, 6707, doi: 10.1021/jp056163x

- Slanger, T. G., Sharpee, B. D., Pejaković, D. A., et al. 2011,
 Atomic oxygen emission intensity ratio: Observation and theory,
 Eos, Transactions American Geophysical Union, 92, 291,
 doi: 10.1029/2011eo350005
- Storey, P. J., & Zeippen, C. J. 2000, Theoretical values for the [OIII] 5007/4959 line-intensity ratio and homologous cases, Monthly Notices of the Royal Astronomical Society, 312, 813, doi: 10.1046/j.1365-8711.2000.03184.x
- Tull, R. G., MacQueen, P. J., Sneden, C., & Lambert, D. L. 1995,
 The High-Resolution Cross-Dispersed Echelle White Pupil
 Spectrometer of the McDonald Observatory 2.7-m Telescope,
 PASP, 107, 251, doi: 10.1086/133548
- Virtanen, P., Gommers, R., Oliphant, T. E., et al. 2020, SciPy 1.0: fundamental algorithms for scientific computing in Python, Nature Medicine, 17, 261, doi: 10.1038/s41592-019-0686-2
- Wang, S.-i., Hildebrand, R. H., Hobbs, L. M., et al. 2003, in Instrument Design and Performance for Optical/Infrared Ground-based Telescopes, ed. M. Iye & A. F. M. Moorwood (SPIE), doi: 10.1117/12.461447
- Werner, M. W., Roellig, T. L., Low, F. J., et al. 2004, The Spitzer Space Telescope Mission, ApJS, 154, 1, doi: 10.1086/422992